Int. J. Solids Structures, 1970, Vol. 6, pp. 757 to 772. Pergamon Press. Printed in Great Britain

STRAIN HARDENING EFFECTS ON UNLOADING SPHERICAL WAVES IN AN ELASTIC PLASTIC MEDIUM

C. Y. YANG

Associate Professor, Civil Engineering Department,
University of Delaware, Newark, Delaware, U.S.A.

Abstract—The propagation of unloading shock waves in an elastic–plastic and strain hardening medium is studied on the basis of the deformation theory of plasticity and the method of characteristics. The load is applied suddenly at the surface of the spherical cavity. The effect of hardening on the decay of the shock strength of principal shearing strains, on the residual strains and the radial normal stresses is shown. A single parameter G_p/G is defined for the quantitative specification of the plastic and linear strain hardening characteristics of the medium.

INTRODUCTION

THE problem of spherical wave propagation in elastic solids has been studied by many researchers. Among the most recent investigators are P. C. Chou and H. A. Koening [1]. For inelastic spherical waves, H. G. Hopkins [2] has published an extensive survey in which important contributions from the United States, Europe and Russia have been reviewed. In particular, a solution by Hunter for an elastic plastic and linear hardening material is explained in detail. Hunter's solution, however, is obtained by an inverse method which is applicable for a particular and restrictive loading. Recently, M. G. Friedman, H. H. Bleich and R. Parnes [3], C. H. Mok [4] and S. K. Garg [5] have obtained solutions for elastic-perfectly plastic shock waves by finite difference methods. S. Kaliski and E. Wlodarczyk [p. 470, 6] investigated unloading waves in a rigid plastic and layered medium. They also studied an elastic–plastic–linear hardening medium but introduced a simplifying assumption of elastic incompressibility [p. 487, 6]. P. Perzyna and J. Bejda [7] investigated a work-hardening and rate sensitive plastic medium which leads to two simple linear formulations for the elastic and plastic range, respectively. The range of applicability of the two formulations is governed by a plasticity criterion which is analogous to the theory of elastic–viscous–plastic waves in bars by V. V. Sokolovsky [8]. In the formulation of Ref. 7, the wave speed in the plastic range is assumed equal to that in the elastic range. In a real material this is generally not the case and consequently the assumption may lead to errors.

In this paper, the propagation of spherical unloading waves in an elastic–plastic, linear hardening material is considered. The source of the waves is a uniform pressure applied on the inner surface of a spherical cavity, Fig. 1. In particular, the effect of hardening on the decay of the plastic shock strength and the residual plastic strain in the medium is investigated in detail. The assumption of elastic incompressibility is not required. The formulation is developed on the basis of the deformation theory† established by A. A. Illyushin [9] and applied by Y. L. Luntz [10]. Luntz, however, did not investigate the strain hardening effect, which is the primary interest of the present work.

† The theory is shown by Illyushin to be applicable to a medium undergoing simple loading or unloading where the ratio between all the applied external forces remains constant with time. This condition is clearly satisfied in the present problem.

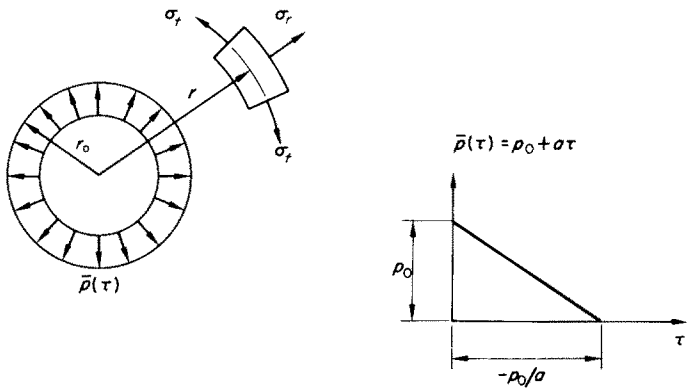

FIG. 1. Spherical cavity and loading.

FORMULATION AND ANALYSIS

It is assumed that the elastic–plastic and hardening property of the medium follows the relation,

$$\sigma = F(\varepsilon) \tag{1}$$

where σ and ε are the generalized stress and strain respectively. The generalized stress and strain are defined in terms of the principal stresses $\sigma_1, \sigma_2, \sigma_3$ and strains, $\varepsilon_1, \varepsilon_2, \varepsilon_3$ by the equations:

$$\sigma = \frac{1}{\sqrt{6}}\sqrt{[(\sigma_1-\sigma_2)^2+(\sigma_2-\sigma_3)^2+(\sigma_3-\sigma_1)^2]} \tag{2}$$

$$\varepsilon = \sqrt{(\tfrac{2}{3})}\sqrt{[(\varepsilon_1-\varepsilon_2)^2+(\varepsilon_2-\varepsilon_3)^2+(\varepsilon_3-\varepsilon_1)^2]}. \tag{3}$$

The function $F(\varepsilon)$ is defined separately for the case of loading and unloading. Since σ and ε are always positive, the stress–strain relation is completely defined in the first quadrant, Fig. 2.

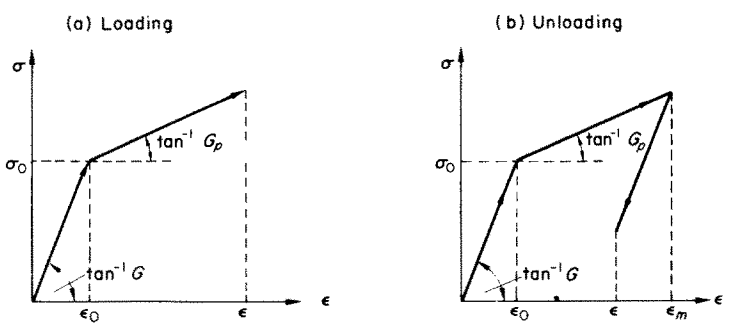

FIG. 2. Generalized stress–strain relation.

Loading

$(\partial\varepsilon/\partial t > 0$, Fig. 2a)

$$\sigma = F(\varepsilon) = G\varepsilon_0 + G_p(\varepsilon - \varepsilon_0),\ \varepsilon \geq \varepsilon_0 > 0 \tag{4}$$

where G and G_p are shear moduli in the elastic and plastic range, respectively, and ε_0 is the generalization strain at yield. When $G_p = G$, equation (4) reduces to the elastic relation $\sigma = G\varepsilon$ and when $G_p = 0$ it reduces to the perfectly plastic relation where the stress is a constant, $G\varepsilon_0$. The generalized stress σ_0 at yield is

$$\sigma_0 = G\varepsilon_0. \tag{5}$$

The value of σ_0 can be obtained from a uniaxial tension test since in that particular case, $\sigma_2 = \sigma_3 = 0$ and

$$\sigma_0 = \sigma_1/\sqrt{3} = \sigma_y/\sqrt{3} \tag{6}$$

where σ_y is the uniaxial tensile stress at yield†.

Unloading

$(\partial\varepsilon/\partial t < 0$, Fig. 2b)

$$\sigma = G\varepsilon + (G_p - G)(\varepsilon_m - \varepsilon_0), \qquad \varepsilon_m \geq \varepsilon > \varepsilon_0 > 0 \tag{7}$$

where ε_m is the maximum generalized strain. When $G_p = 0$ equation (7) reduces to the perfectly plastic case with no hardening,

$$\sigma = G(\varepsilon + \varepsilon_0 - \varepsilon_m), \qquad \varepsilon_m \geq \varepsilon > \varepsilon_0 > 0.$$

For many real materials, especially metals, one can restrict considerations to values of G such that $0 < G_p < G$.

Spherical unloading (Fig. 3)

$$\sigma = (\sigma_t - \sigma_r)/\sqrt{3}, \qquad \varepsilon = 2(\varepsilon_t - \varepsilon_r)/\sqrt{3}.$$

Let the principal shearing strains θ, θ_0 and θ_m be defined as

$$\theta = (\varepsilon_t - \varepsilon_r), \qquad \theta_0 = (\varepsilon_t - \varepsilon_r)_0, \qquad \theta_m = (\varepsilon_t - \varepsilon_r)_m \tag{8}$$

where the subscripts 0 and m denote yield strain and maximum strain, respectively‡. Equation (7) for unloading becomes

$$(\sigma_t - \sigma_r) = 2G\theta + 2(G_p - G)(\theta_m - \theta_0), \qquad \theta_m \geq \theta > \theta_0 > 0. \tag{9}$$

Note that equations (7) and (9) assume elastic unloading from a plastic state as indicated by the inequalities for ε and θ.

At the yield limit, from equation (3),

$$\varepsilon_0 = 2(\varepsilon_t - \varepsilon_r)_0/\sqrt{3}.$$

† According to Mises' theory [11], σ_y equals $\sqrt{(3)}k$, where k is the yield limit in simple shear, so that $\sigma_0 = k$. According to Tresca $\sigma_y = 2k$ so that $\sigma_0 = 2k/\sqrt{3}$ [11].

‡ See Ref. 11, p. 17.

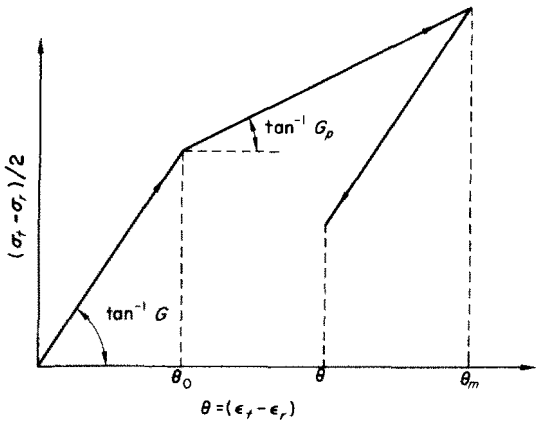

FIG. 3. Stress–strain relation of unloading in spherical symmetric case.

From the above equation and equations (8) and (5) it follows that at the yield limit,

$$\theta_0 = (\varepsilon_t - \varepsilon_r)_0 = \sqrt{(3)}\varepsilon_0/2 = \sqrt{(3)}\sigma_0/2G. \tag{10}$$

In addition to the stress–strain relation, equation (9), applicable in the plastic range for spherical unloading, the combined condition of plastic incompressibility and volumetric law of elastic deformation is assumed, that is

$$2\sigma_t + \sigma_r = 3K(2\varepsilon_t + \varepsilon_r). \tag{11}$$

The equation of motion is

$$\rho\frac{\partial^2 u}{\partial t^2} = \frac{\partial \sigma_r}{\partial r} + 2\frac{(\sigma_r - \sigma_t)}{r} \tag{12}$$

where K is the bulk modulus, ρ density, u radial displacement, r radial coordinate and t time.

Dynamic formulation

Equations (9), (11) and (12) constitute a complete system for the elastic–plastic unloading waves. It is convenient for the solution of boundary value problems to combine the three equations into one for the displacement, u. Substitution of $(\varepsilon_t - \varepsilon_r)$ for θ in equation (9) and then u/r for ε_t and $\partial u/\partial r$ for ε_r in equation (9) and equation (11) yields two equations in σ_t, σ_r and u. From these two equations expressions for σ_t, σ_r and $\partial\sigma_r/\partial r$ in terms of u can be obtained. Substitution of these expressions into equation (12) yields

$$\frac{\partial^2 u}{\partial r^2} + \frac{2}{r}\frac{\partial u}{\partial r} - 2\frac{u}{r^2} = \frac{I}{c^2}\frac{\partial^2 u}{\partial t^2} + h\left[\frac{\mathrm{d}\theta_m}{\mathrm{d}r} + \frac{3(\theta_m - \theta_0)}{r}\right] \tag{13a}$$

where

$$h = (c_p^2 - c^2)/c^2 \tag{13b}$$

$$c = \sqrt{[(4G+3K)/3\rho]} = \text{elastic speed wave} \tag{13c}$$

$$c_p = \sqrt{[(4G_p+3K)/3\rho]} = \text{plastic wave speed}\dagger. \tag{13d}$$

† This can be obtained from the dynamic formulation for loading in which equation (7) is replaced by equation (4).

Let

$$\bar{\theta} = \theta/\theta_0, \qquad \bar{\theta}_m = \theta_m/\theta_0, \qquad \bar{u} = u/r_0\theta_0, \qquad \tau = ct/r_0 \quad \text{and} \quad \bar{r} = r/r_0$$

where r_0 is the radius of the cavity.
Then

$$\frac{\partial^2 \bar{u}}{\partial \bar{r}^2} + \frac{2}{\bar{r}}\frac{\partial \bar{u}}{\partial \bar{r}} - 2\frac{\bar{u}}{\bar{r}^2} = \frac{\partial^2 \bar{u}}{\partial \tau^2} + h\left[\frac{\mathrm{d}\bar{\theta}_m}{\mathrm{d}\bar{r}} + \frac{3(\bar{\theta}_m - 1)}{\bar{r}}\right]. \tag{14}$$

This is the dynamic equation for the elastic–plastic unloading waves with linear hardening. When $c_p = c$, $h = 0$, equation (14) reduces to the familiar equation for elastic spherical waves.

Characteristics and wave fronts

The only type of loading considered here is a pressure applied uniformly on the cavity surface. The applied pressure has a finite jump at $\tau = 0$ and decreases monotonically in time, Fig. 1. For this loading the wave fronts in the Lagrangian plane can be determined *a priori* on the basis of the theory of characteristics, as follows:

The various wave fronts can be explained most clearly when the problem of a continuous pressure, Fig. 4(a), is considered first. The jump in pressure at $\tau = 0$ then can be obtained by a limiting procedure, Fig. 4(b). In Fig. 4(a), a continuous pressure vs. time diagram is plotted on the left side of the $\bar{r}$–τ plane. At $\tau = 0$ a leading elastic wave is propagated into the medium with speed c. The locus of this wave is the characteristic line ab defined by the equation, $\bar{r} - 1 = \tau$. After a certain time when the pressure increases to such a magnitude as to initiate yielding, a plastic wave will propagate with speed c_p. Plastic

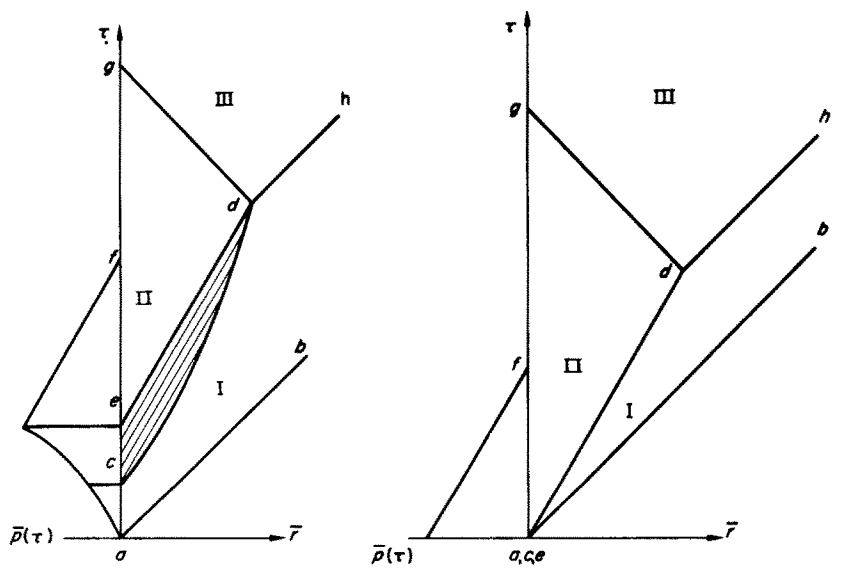

FIG. 4. Wave fronts in $\bar{r}$–τ plane.

waves will propagate from the cavity from the time of initial yielding, say at the point c in Fig. 4(a), through the time of initial unloading at the point e. The curve cd and the point d which define the elastic–plastic interface and the extent of plastic deformation can not be determined *a priori*. The characteristic line ed with slope c_p/c is the locus of the plastic wave prior to unloading. The lines parallel to ed represent plastic waves with gradually varying depths of propagation. Therefore, the region $abcdh$ bounded by the leading elastic wave front ab, the time interval ac, the elastic–plastic interface cd and the elastic characteristic dh, is the first elastic region. The region cde bounded by the elastic–plastic interface cd, the time interval ce and the plastic wave ed is the plastic region. The region egd bounded by the elastic characteristic dg, the time interval eg and the plastic wave ed is the second elastic region. The region above the characteristics dg and dh is the third elastic region and is not of primary interest because of the long time after the peak load.

The wave fronts for the problem with pressure jump at $\tau = 0$, Fig. 4(b), can now be determined. This is accomplished by decreasing the time interval ae in Fig. 4(a) to zero, so that the plastic region cde is reduced to a limiting line ad. The line ad is therefore both the plastic wave front and the elastic–plastic interface. The $\bar{r}$–τ plane is divided into four regions, the undisturbed region $ab\bar{r}$ ahead of the leading elastic front and the three elastic regions $abdh$, agd and the region above lines dg and dh. The plastic wave front ad is determined *a priori* as a characteristic with slope c_p/c. The point d representing the depth of plastic deformation, however, is not known and must be determined along with the other unknowns of a problem.

Boundary conditions

Along the leading elastic front ab, Fig. 4(b), $\bar{u} = 0$. Along the plastic wave front ad, $\bar{u} = g(\bar{r})$ which is the displacement $\bar{u}(\bar{r}, \tau)$ evaluated along ad. The function $g(\bar{r})$ is known, once the solution in the first elastic region is obtained. The principal shearing strain $\bar{\theta} = 1$ at the instant the plastic wave arrives at a position along ad, and jumps to $\bar{\theta}_m \geq 1$ immediately before unloading. At the cavity surface $\bar{\sigma}_r = \bar{p}(\tau)$ and along $\tau = 0$, $\bar{u} = \bar{u}_\tau = 0$. Both $\bar{\sigma}_r$ and $\bar{p}$ are non-dimensionalized by the quantity $\rho c^2 \theta_0$. All the boundary conditions are shown in Fig. 5.

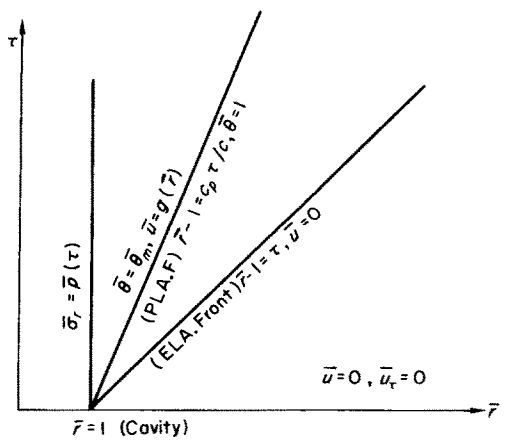

FIG. 5. Boundary conditions.

Solution in region I

In the first elastic region ahead of the plastic wave the governing equation is

$$\frac{\partial^2 \bar{u}}{\partial \bar{r}^2}+\frac{2}{\bar{r}}\frac{\partial \bar{u}}{\partial \bar{r}}-2\frac{\bar{u}}{\bar{r}^2}=\frac{\partial^2 \bar{u}}{\partial \tau^2}. \tag{15}$$

A closed form solution satisfying the boundary conditions shown in Fig. 5 was obtained by Luntz [p. 65, 10] as follows;

$$\bar{u}(\bar{r},\tau)=\frac{1}{(\lambda-1)(6\lambda-3)}\left\{\frac{\lambda}{\bar{r}}\left[-3\xi^2+\xi^{\mu-1}\left(\cos(v\ln\xi)+\frac{3\mu-v^2-\mu^2}{v}\sin(v\ln\xi)\right)\right]\right.$$

$$\left.-\frac{1}{\bar{r}^2}\left[-\xi^3+\xi^{\mu}\left(\cos(v\ln\xi)+\frac{3-\mu}{v}\sin(v\ln\xi)\right)\right]\right\} \tag{16}$$

where

$$\xi=\lambda(\bar{r}-\tau-1)+1, \qquad \lambda=\frac{c_p}{c_p-c}$$

$$\mu=\frac{\lambda+3}{2\lambda}, \qquad v=\frac{-\sqrt{[12-(\lambda+3)^2]}}{2\lambda}.$$

The displacement along the plastic wave front *ad*, Fig. 4(b), defined by $\bar{r}=1+(c_p\tau/c)$, may be obtained from equation (16) as,

$$\bar{u}(\bar{r})=g(\bar{r})=\frac{1}{(\lambda-1)(6\lambda-3)}\left\{(-3\lambda+1)\bar{r}+r^{\mu-2}\right.$$

$$\left.\times\left[(3\lambda-1)\cos(v\ln\bar{r})+\frac{3\lambda^2+4\lambda-3}{2\lambda v}\sin(v\ln\bar{r})\right]\right\}. \tag{17}$$

Solution in region II

The governing equation equation (14) derived earlier is assembled here with the boundary conditions obtained from the continuity of displacements and equations (9) and (11).

$$\frac{\partial^2 \bar{u}}{\partial \bar{r}^2}+\frac{2}{\bar{r}}\frac{\partial \bar{u}}{\partial \bar{r}}-2\frac{\bar{u}}{\bar{r}^2}=\frac{\partial^2 \bar{u}}{\partial \tau^2}+h\left[\frac{\mathrm{d}\theta_m}{\mathrm{d}\bar{r}}+\frac{3(\bar{\theta}_m-1)}{\bar{r}}\right] \tag{18}$$

$$\bar{u}(\bar{r},\tau)=\bar{u}(\bar{r})=g(\bar{r}), \text{ along } \bar{r}=1+c_p\tau/c \tag{19}$$

$$\frac{\partial \bar{u}}{\partial \bar{r}}+\left(\frac{3K}{\rho c^2}-1\right)\bar{u}-\frac{4}{3\rho c^2}(G_p-G)(\bar{\theta}_m-1)=\frac{1}{\rho c^2\theta_0}p(t)=\bar{p}(\tau), \qquad \text{along } \bar{r}=1. \tag{20}$$

Let

$$\bar{u}(\bar{r},\tau)=U(\bar{r},\tau)+v(\bar{r}) \tag{21}$$

where $v(\bar{r})$ satisfies the following inhomogeneous ordinary differential equation and the two boundary conditions:

$$\frac{d^2v}{d\bar{r}^2}+\frac{2}{\bar{r}}\frac{dv}{d\bar{r}}-\frac{2v}{\bar{r}^2}=h\left(\frac{d\bar{\theta}_m}{d\bar{r}}+\frac{3(\bar{\theta}_m-1)}{\bar{r}}\right) \tag{22}$$

$$\frac{dv}{d\bar{r}}-\frac{v}{\bar{r}}=h(\bar{\theta}_m-1), \qquad \text{at } \bar{r}=1+c_p\tau/c \tag{23†}$$

$$v=0, \qquad \text{at } \bar{r}=1. \tag{24}$$

Substituting $\bar{u}(\bar{r},\ \tau)$ into equations (18), (19) and (20) and making use of the equations (22), (23) and (24) yields the governing equations for $U(\bar{r},\tau)$,

$$\frac{\partial^2U}{\partial\bar{r}^2}+\frac{2}{\bar{r}}\frac{\partial U}{\partial\bar{r}}-\frac{2U}{\bar{r}^2}=\frac{\partial^2U}{\partial\tau^2} \tag{25}$$

$$\frac{\partial U}{\partial\bar{r}}+\frac{c_p}{c}\frac{\partial U}{\partial\tau}-\frac{U}{r}=f(\bar{r})‡ \qquad \text{along } \bar{r}=1+c_p\tau/c \tag{26}$$

$$\frac{\partial U}{\partial\bar{r}}+\left(\frac{3K}{\rho c^2}-1\right)U=\bar{p}(\tau), \qquad \text{along } \bar{r}=1 \tag{27}$$

where

$$f(\bar{r})=h\{1+a\bar{r}^{\mu-3}[\cos(\nu\ln\bar{r})+b\sin(\nu\ln\bar{r})]\} \tag{28}$$

$$a=\frac{\lambda}{1-2\lambda}, \qquad b=\frac{2\lambda^2+\lambda-1}{2\lambda\nu(2\lambda-1)}.$$

The problem now is to construct solutions for $U(\bar{r},\tau)$. This is accomplished by the method of characteristics. The characteristic lines and the corresponding compatibility equations are given as follows (see equation 10 [12]):

$$d\bar{r}=d\tau, \qquad dU_\tau=dU_{\bar{r}}+2\left(\frac{U_{\bar{r}}}{\bar{r}}-\frac{U}{\bar{r}^2}\right)d\tau \tag{29}$$

$$d\bar{r}=-d\tau, \qquad dU_\tau=-dU_{\bar{r}}+2\left(\frac{U_{\bar{r}}}{\bar{r}}-\frac{U}{\bar{r}^2}\right)d\tau \tag{30}$$

where the subscripts $\bar{r}$ and τ denote partial derivatives. On the basis of these ordinary differential equations (29) and (30), the boundary conditions equations (26) and (27) and the equation, $dU=U_{\bar{r}}\,d\bar{r}+U_\tau\,d\tau$, solutions for the functions U, $U_{\bar{r}}$ and U_τ can be obtained by a usual numerical procedure. Some explanation will be given in the next section.

Once the function $U(\bar{r},\tau)$ is constructed, the function $v(\bar{r})$ can be computed from equation (21) written along the plastic wave front, i.e.

$$v(\bar{r})=g(\bar{r})-U(\bar{r},\tau), \qquad \text{along } \bar{r}=1+c_p\tau/c,$$

where $g(\bar{r})$ is the known solution for displacements in equation (19). The construction of the solution for $\bar{u}(\bar{r},\tau)$ is now complete.

† First of equations (23) applies everywhere in the region. This may be verified upon differentiation and then subtraction from equation (22).

‡ Some details in the derivation of this equation are given in Appendix A.

NUMERICAL PROBLEMS

A set of numerical problems is used to study the effect of strain hardening on the propagation of plastic shock waves, the residual strains and the radial normal stresses in the medium. The applied load has a jump at $\tau = 0$ and decreases linearly with time, Fig. 1. The elastic Poisson's ratio σ' is selected to be $\frac{1}{4}$, so that

$$\frac{4G}{3K} = \frac{2(1-2\sigma')}{1+\sigma'} = 0{\cdot}8,$$

and

$$\frac{G_p}{G} = \frac{4G_p/3K}{0{\cdot}8}.$$

Also from equations (13)

$$\frac{c}{c_p} = \sqrt{\left(\frac{4G+3K}{4G_p+3K}\right)} = \sqrt{\left[\frac{1{\cdot}8}{1+(4G_p/3K)}\right]}. \tag{31}$$

The only independent parameter therefore is the strain-hardening parameter G_p/G. For convenience a list of problems with given data is shown in Table 1.

TABLE 1. DATA USED IN PROBLEMS (POISSON'S RATIO $\sigma' = 0{\cdot}25$)

Prob. no.	Load†		Hardening parameter	Ratio of wave speeds	Network size Fig. 6		
	p_0	a	G_p/G	c/c_p	$\Delta\bar{r}_1$	$\Delta\tau_1$	$\Delta\bar{r} = \Delta\tau$
1	−1·2	2·4	0	1·342	0·020	0·0268	0·0234
2	−1·2	2·4	0·100	1·291	0·020	0·0258	0·0229
3	−1·2	2·4	0·187	1·251	0·020	0·0250	0·0225
4	−1·2	2·4	0·262	1·220	0·020	0·0244	0·0222
5	−1·2	2·4	0·313	1·200	0·020	0·0240	0·0220

† For results shown in Figs. 9–12 the p_0 values are changed as indicated.

The computation is a simple numerical integration technique applied along characteristics for the functions U, $U_{\bar{r}}$ and U_τ. Referring to Fig. 6 for the characteristic network it is clear that once the net size $\Delta\bar{r}_1$ is selected the complete net is defined by the plastic front with slope c_p/c and the 45° lines. The computational procedure starts from the solution of the initial three points, Fig. 6 points $(1, 0)$, $(1+\Delta\bar{r}_1, \Delta\tau_1)$ and $(1, 2\Delta\tau)$ using formulas given in Appendix B. The rest of the node points are then treated systematically with the help of a set of new coordinate axes at 45° with the original $(\bar{r}, \tau)$ set. These node points are classified into four types; points on the plastic front, points next to the front, points on the cavity surface and interior regular points. On the plastic front solutions for the three unknowns U, $U_{\bar{r}}$ and U_τ are determined from the boundary condition equation (26), a condition equation (29) along a backward-drawn characteristic, and the differential condition $dU = U_{\bar{r}}\,d\bar{r} + U_\tau\,d\tau$. This differential condition, of course, applies to all four types of points so only two additional conditions are required. On the cavity

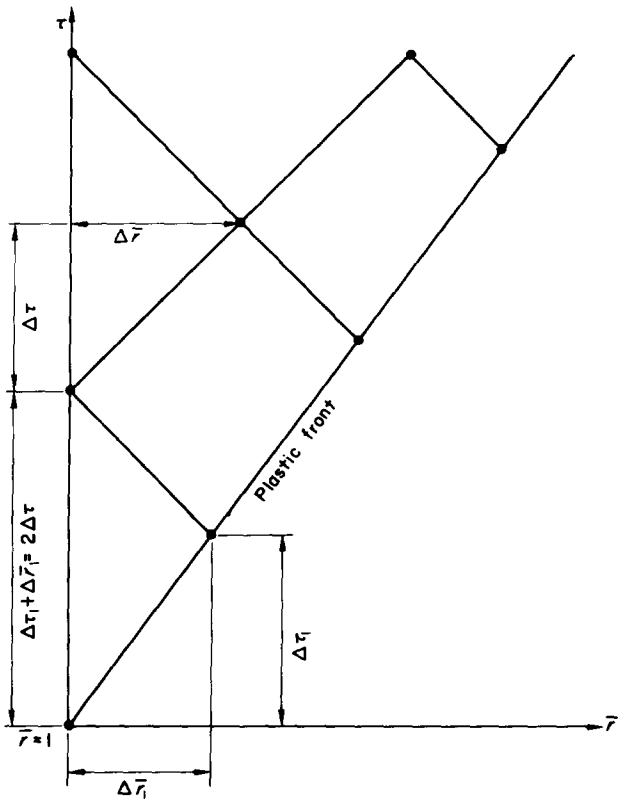

FIG. 6. Characteristic network.

surface these are the boundary conditions of equation (27) and a condition in equation (30) along a backward-drawn characteristic. For interior regular points located on top of a right diamond-shaped net, the two characteristic conditions equations (29) and (30) apply. Due to the irregular geometry of nets near the plastic front, Fig. 6, a backward-drawn characteristic at the front always intersects another characteristic at a point which is not a node and therefore unknowns at this intersection must be obtained by interpolation. Furthermore, points next to the front have a backward-drawn characteristic of a different length. The length is determined by the slope of the plastic front. Actual computations were programmed in FORTRAN language and carried out on an IBM 7094 computer.

The most important result is the maximum principal shearing strain $\bar{\theta}_m$ along the plastic shock front. The quantity can be computed as follows once the functions U, $U_{\bar{r}}$ are obtained. From equations (8), (21) and (23),

$$\bar{\theta}_m = \frac{\bar{u}}{\bar{r}} - \frac{\partial \bar{u}}{\partial \bar{r}} = \left(\frac{U}{\bar{r}} - U_{\bar{r}}\right) + \left(\frac{v}{\bar{r}} - \frac{\mathrm{d}v}{\mathrm{d}\bar{r}}\right) = \left(\frac{U}{\bar{r}} - U_{\bar{r}}\right) + h(1-\bar{\theta}_m)$$

$$\therefore \quad \bar{\theta}_m = 1 + \left(\frac{c}{c_p}\right)^2 \left(\frac{U}{\bar{r}} - U_{\bar{r}} - 1\right). \tag{32}$$

The residual principal shearing strain $\bar{\theta}_r$ can be obtained by letting $(\sigma_t - \sigma_r)/2 = 0$ in equation (9) and dividing all terms by $\bar{\theta}_0$. Thus,

$$\bar{\theta}_r = \left(1 - \frac{G_P}{G}\right)(\bar{\theta}_m - 1). \tag{33}$$

The radial normal stress $\bar{\sigma}_r$ can be computed from equation (20) with $\bar{u}$ replaced by $\bar{u}/\bar{r}$ and $p(t)$ by σ_r. Since $\theta_0 = \sigma_y/2G$ and $c^2 = (4G+3K)/3\rho$ it follows that for Poisson's ratio $\sigma' = \frac{1}{4}$,

$$\bar{\sigma}_r = \frac{\sigma_r}{\rho c^2 \theta_0} = \frac{2}{3}\frac{\sigma_r}{\sigma_y} \tag{34}$$

where σ_y is the uniaxial tensile stress at yield. Thus, the nondimensional radial normal stress $\bar{\sigma}_r$ (and the applied load $\bar{p}$ which is $\bar{\sigma}_r$ at $\bar{r} = 1$) may take either of the two ratios.

DISCUSSION OF RESULTS

The most important results of this investigation are presented in Figs. 7–12. Figure 7 is a plot of the maximum principal shearing strain, $\bar{\theta}_m$ at the plastic wave front vs. the wave front position, $\bar{r}$. The strain $\bar{\theta}$ at this front has a jump from the yield limit of unity to the maximum $\bar{\theta}_m$. From Fig. 7, it can be seen that the strength $\delta\bar{\theta}_m = \bar{\theta}_m - 1$ of the jump or shock decays almost linearly as it is propagated into the medium with the plastic wave speed c_p. Three curves are shown in Fig. 7. The upper one in the figure corresponds to an ideal plastic medium with no strain hardening effect, $G_p/G = 0$. The lower one corresponds to a medium with strong hardening effect, $G_p/G = 0{\cdot}313$. Consequently, it can be seen that the effect of hardening on the decay of the shock strength $\delta\bar{\theta}_m$ at the cavity surface is approximately from 0·36 to 0·29. The extent of the plastic region $\bar{r}$ is from 1·18 to about 1·19.

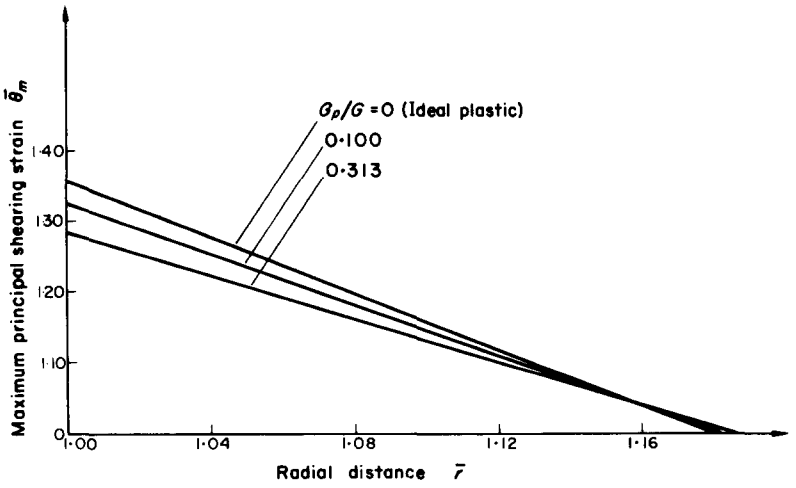

FIG. 7. Maximum principal shearing strain. Prob. 1, 3, 5.

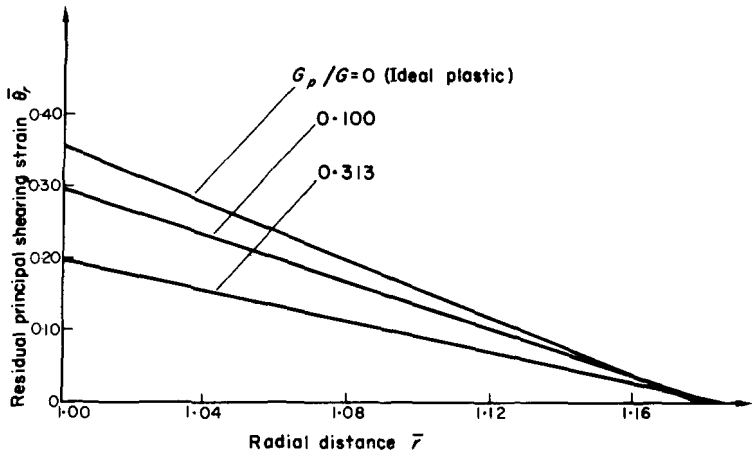

FIG. 8. Residual principal shearing strain. Prob. 1, 3, 5.

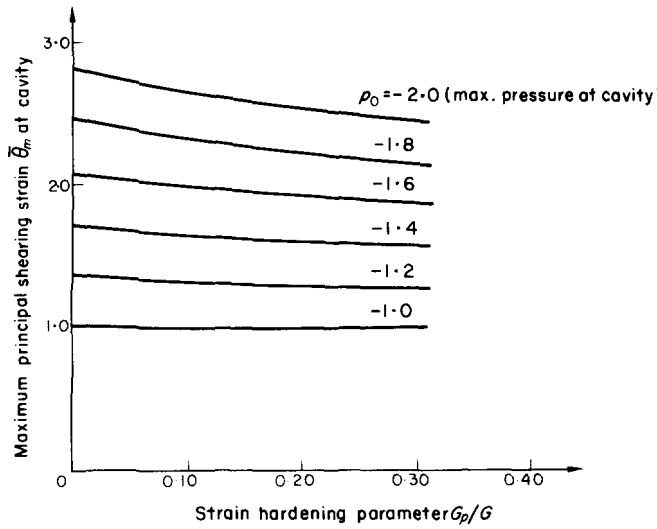

FIG. 9. Maximum principal shearing strain at cavity. Prob. 1, 2, 3, 4, 5.

Figure 8 is a plot of the residual principal shearing strain $\bar{\theta}_r$ vs. the radial distance $\bar{r}$. The effect of strain hardening on the magnitude of the residual strain $\bar{\theta}_r$ is quite significant, from 0·36 in the ideal plastic medium to 0·20 at the cavity surface in a medium with a strong hardening effect. The results in Figs. 7 and 8 are all for a linearly decreasing pressure, Fig. 1, with $p_0 = -1{\cdot}2$ and $a = 2{\cdot}4$.

For unloading situations with higher magnitudes of p_0, the maximum principal shearing strain $\bar{\theta}_m$ at the cavity surface is plotted against the parameter of strain hardening in Fig. 9. The residual principal shearing strain $\bar{\theta}_r$ is plotted in Fig. 10.

Figures 11 and 12 show the spatial distribution of the radial normal stress $\bar{\sigma}_r$ at two different times for the ideal elastic–plastic medium, $Gp/G = 0$, and for a strong hardening medium, $Gp/G = 0{\cdot}313$, respectively. The effect of hardening on the magnitudes of $\bar{\sigma}_r$

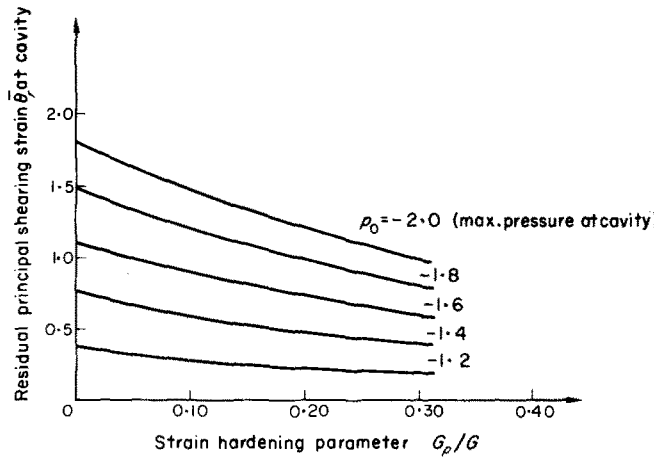

FIG. 10. Residual principal shearing strain at cavity. Prob. 1, 2, 3, 4, 5.

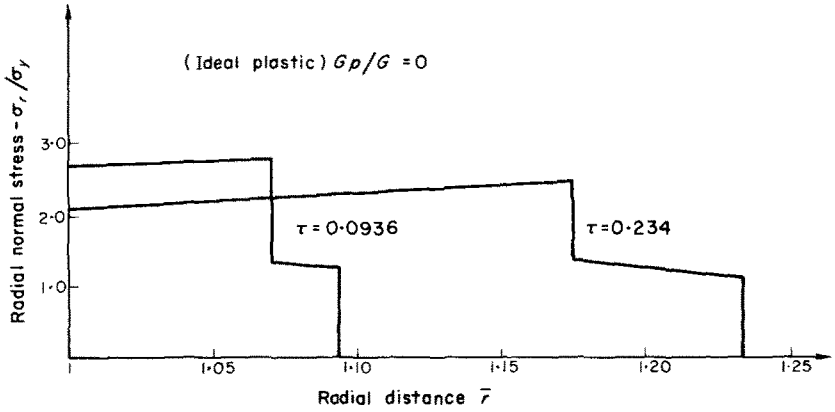

FIG. 11. Radial normal stress problem 1 with $p_0 = -2·0$.

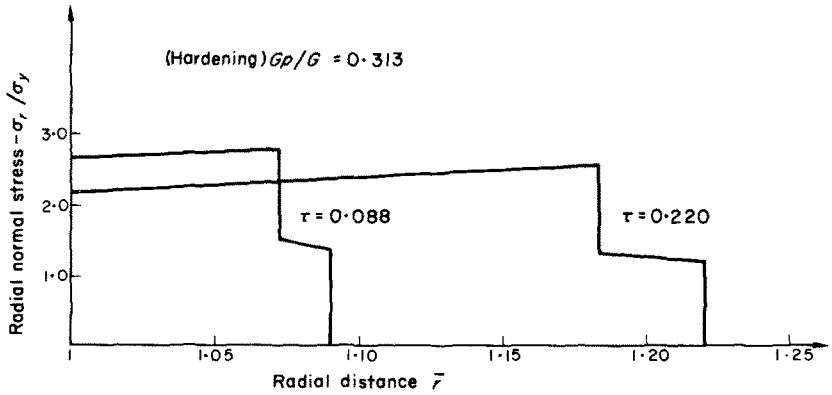

FIG. 12. Radial normal stress problem 5 with $p_0 = -2·0$.

is not significant. The radial distance between the leading elastic front and the plastic front is considerably shortened in the hardening case as expected on theoretical grounds. It is interesting to note the recent work by C. H. Mok [Fig. 2(a), 4] on a finite difference solution for an ideal elastic–plastic medium under a constant pressure. The numerical solution for the spatial distribution of radial normal stress $\bar{\sigma}_r$ appears to be satisfactory in several comparison studies made by the author. However, as pointed out in that paper [p. 375, 4], the existence of a discontinuity at the elastic–plastic boundary is not clear. Such a discontinuity is shown very definitely in Figs. 11 and 12 here. The spatial variation of $\bar{\sigma}_r$ behind the plastic front as shown here is quite different from those shown by Mok [Fig. 2(a), 4] primarily due to the difference of load applied. This statement is supported by a comparison of the work by M. G. Friedman, H. H. Bleich and R. Parnes [Fig. 7, 3] where the applied load at the cavity surface decreases exponentially with time. Furthermore, another recent work for an ideal elastic–plastic medium by S. K. Garg [Fig. 1, 5] also shows similar behavior for $\bar{\sigma}_r$ for a load with initial constant and later decreasing magnitudes. This initial constant load introduces a plastic region for $\bar{\sigma}_r$ which separates the unloading region from the elastic-precursor [Fig. 1, 5]. For other main features of $\bar{\sigma}_r$ including the discontinuities at the elastic and plastic fronts and the spherical divergence of the progressing waves, results obtained here for the ideal elastic–plastic medium agree in general with those of References [3] and [5].

CONCLUSIONS

The strain hardening property for an elastic–plastic medium can be defined by a parameter G_p/G. For a wide range of this parameter and for the unloading wave studied, the following conclusions can be made.

1. The maximum principal shearing strain $\bar{\theta}_m$ and the shock $\delta\bar{\theta}_m$ at the plastic wave front decrease somewhat with increasing strain hardening.
2. The extent of plastic region increases slightly with increasing strain hardening.
3. The residual principal shearing strain $\bar{\theta}_r$ decreases significantly with increasing strain hardening.
4. The distance between the elastic and plastic fronts of the radial normal stresses decreases with increasing hardening but the effect on the magnitudes of the stresses is not significant.

Acknowledgment—This study was supported in part by the Office of Naval Research under Contract Nonr 1834-(03) with the Civil Engineering Department, University of Illinois and by a research grant (2-970-791) from the University of Delaware Research Foundation.

REFERENCES

[1] P. C. CHOU and H. A. KOENING, *J. appl. Mech.* **33**, 159–167 (1966).
[2] H. G. HOPKINS, *Progress in Solid Mechanics*, Vol. 1, pp. 85–163. North-Holland (1960).
[3] M. G. FRIEDMAN, H. H. BLEICH and R. PARNES, *Proc. Am. Soc. Civ. Engrs* **91**, EM3, 189–203 (1965).
[4] C. H. MOK, *J. appl. Mech.* **33**, 372–378 (1968).
[5] S. K. GARG, *J. appl. Math Phys.* **19**, 243–251 (1968).
[6] S. KALISKI and E. WŁODARCZYK, *Nonlinear Vib. Prob.* **5**, 469–492 (1963).

[7] P. PERZYNA and J. BEJDA, *Bull. acad. Pol. Sci., Sér. Sci. Techn.* **12**, 233–283 (1964).
[8] V. V. SOKOLOVSKY, *Akad. Nauk SSSR, Prikl. Math. Mech.* (in Russian) **12**, (1948).
[9] A. A. ILLYUSHIN and V. S. LENSKY, *Strength of Materials* (English translation). Pergamon Press (1967).
[10] Y. L. LUNTZ, *Akad. Nauk SSSR, Prikl. Math. Mech.* (in Russian) **13**, 55–78 (1949).
[11] W. PRAGER and P. G. HODGE, JR., *Theory of Perfectly Plastic Solids*, p. 24. Wiley (1951).
[12] P. C. CHOU and R. W. MORTIMER, *J. appl. Mech.* **34**, 745–750 (1967).

APPENDIX

A. Derivation of equation (26)

Along the plastic wave front, $\bar{r} = 1 + c_p\tau/c$, the following conditions hold. From equation (19) and (21),

$$\bar{u} = U + v = g(\bar{r})$$

$$\therefore \quad U = g(\bar{r}) - v \tag{A1}$$

$$\frac{U}{\bar{r}} - \frac{\partial U}{\partial \bar{r}} = \left(\frac{\bar{u}}{\bar{r}} - \frac{\partial \bar{u}}{\partial \bar{r}}\right) - \left(\frac{v}{\bar{r}} - \frac{\mathrm{d}v}{\mathrm{d}\bar{r}}\right).$$

From equation (23)

$$\frac{\mathrm{d}v}{\mathrm{d}\bar{r}} - \frac{v}{\bar{r}} = h\left[\frac{\bar{u}}{\bar{r}} - \frac{\partial \bar{u}}{\partial \bar{r}} - 1\right]$$

$$\therefore \quad \frac{U}{\bar{r}} - \frac{\partial U}{\partial \bar{r}} = 1 + \frac{c_p^2}{c_p^2 - c^2}\left(\frac{\mathrm{d}v}{\mathrm{d}\bar{r}} - \frac{v}{\bar{r}}\right) \tag{A2}$$

Taking the differential $\mathrm{d}\bar{u}$ along the wave front where $\mathrm{d}\tau/\mathrm{d}\bar{r} = c/c_p$ yields

$$\mathrm{d}\bar{u} = \frac{\partial \bar{u}}{\partial \bar{r}}\mathrm{d}\bar{r} + \frac{\partial \bar{u}}{\partial \tau}\mathrm{d}\tau = \frac{\partial U}{\partial \bar{r}}\mathrm{d}\bar{r} + \frac{\partial U}{\partial \tau}\mathrm{d}\tau + \frac{\mathrm{d}v}{\mathrm{d}\bar{r}}\mathrm{d}\bar{r}$$

$$\therefore \quad \frac{\partial \bar{u}}{\partial \bar{r}} + \frac{\partial \bar{u}}{\partial \tau}\left(\frac{c}{c_p}\right) = \frac{\partial U}{\partial \bar{r}} + \frac{\partial U}{\partial \tau}\left(\frac{c}{c_p}\right) + \frac{\mathrm{d}v}{\mathrm{d}\bar{r}}.$$

But $\bar{u} = g(\bar{r})$

$$\therefore \quad \frac{\partial U}{\partial \bar{r}} + \frac{c}{c_p}\frac{\partial U}{\partial \tau} + \frac{\mathrm{d}v}{\mathrm{d}\bar{r}} = \frac{\mathrm{d}}{\mathrm{d}\bar{r}}g(\bar{r}). \tag{A3}$$

Eliminating v and $\mathrm{d}v/\mathrm{d}\bar{r}$ from (A1), (A2) and (A3) yields

$$\frac{\partial U}{\partial \bar{r}} + \frac{c_p}{c}\frac{\partial U}{\partial \tau} - \frac{U}{\bar{r}} = h\left\{1 + \frac{c_p^2}{c_p^2 - c^2}\left[\frac{\mathrm{d}}{\mathrm{d}r}g(\bar{r}) - g(\bar{r})/\bar{r}\right]\right\}. \tag{A4}$$

Differentiating $g(\bar{r})$ in equation (17) with $\bar{r}$, then subtracting $g(\bar{r})/\bar{r}$ from it and substituting the result into equation (A4) yields

$$\frac{\partial U}{\partial \bar{r}} + \frac{c_p}{c}\frac{\partial U}{\partial \tau} - \frac{U}{\bar{r}} = f(\bar{r}).$$

B. *Initial three points*

The first point $(1, 0)$:

$$U = 0, \qquad U_{\bar{r}} = p_0, \qquad U_\tau = \frac{c}{c_p}[f(1) - p_0]$$

$$U_{\bar{r}\tau} = a + \left(1 - \frac{3K}{\rho c^2}\right) U_\tau.$$

Taking the derivative of equation (26) along the wave front direction, say s, yields,

$$\frac{\mathrm{d}U_{\bar{r}}}{\mathrm{d}s} + \frac{c_p}{c}\frac{\mathrm{d}U_\tau}{\mathrm{d}s} - \frac{\mathrm{d}}{\mathrm{d}s}\frac{U}{\bar{r}} = \frac{\mathrm{d}f}{\mathrm{d}s}$$

$$\left(U_{\bar{r}\bar{r}}\frac{\mathrm{d}\bar{r}}{\mathrm{d}s} + U_{\bar{r}\tau}\frac{\mathrm{d}\tau}{\mathrm{d}s}\right) + \frac{c_p}{c}\left(U_{\tau\bar{r}}\frac{\mathrm{d}\bar{r}}{\mathrm{d}s} + U_{\tau\tau}\frac{\mathrm{d}\tau}{\mathrm{d}s}\right) - \frac{1}{\bar{r}}\left(U_{\bar{r}}\frac{\mathrm{d}\bar{r}}{\mathrm{d}s} + U_\tau\frac{\mathrm{d}\tau}{\mathrm{d}s}\right) + \frac{U}{\bar{r}^2}\frac{\mathrm{d}r}{\mathrm{d}s} = f'(1)\frac{\mathrm{d}\bar{r}}{\mathrm{d}s}$$

$$\therefore \quad U_{\bar{r}\bar{r}} + U_{\bar{r}\tau}\left(\frac{c}{c_p} + \frac{c_p}{c}\right) + U_{\tau\tau} - \frac{c}{c_p}U_\tau = f'(1). \tag{B1}$$

Combining equation (25) with (B1) yields,

$$U_{\bar{r}\bar{r}} = \left[f'(1) - U_{\bar{r}} + \frac{c}{c_p}U_\tau - \left(\frac{c}{c_p} + \frac{c_p}{c}\right)U_{\bar{r}\tau}\right]/2$$

$$U_{\tau\tau} = U_{\bar{r}\bar{r}} + 2U_{\bar{r}}.$$

The functions U, $U_{\bar{r}}$ and U_τ at the second point $(1 + \Delta\bar{r}_1, \Delta\tau_1)$ and the third point $(1, 2\Delta\tau)$ can be computed by a Taylor's series approximation as follows

$$U = (U_{\bar{r}})_1(\bar{r} - 1) + (U_\tau)_1\tau + (U_{\bar{r}\bar{r}})_1\frac{(\bar{r} - 1)^2}{2} + (U_{\bar{r}\tau})_1\tau(\bar{r} - 1) + (U_{\tau\tau})_1\frac{\tau^2}{2}$$

$$U_{\bar{r}} = (U_{\bar{r}})_1 + (U_{\bar{r}\bar{r}})_1(\bar{r} - 1) + (U_{\bar{r}\tau})_1\tau$$

$$U_\tau = (U_\tau)_1 + (U_{\bar{r}\tau})_1(\bar{r} - 1) + (U_{\tau\tau})_1\tau.$$

(*Received* 24 *June* 1968; *revised* 21 *July* 1969)

Абстракт—На основе деформационной теории пластичности и метода характеристик, исследуется распространение ударных волн в упруго-пластической среде с упрочнением. Нагрузка приложена внезапно на поверхности сферической полости. Указывается влияние эффекта упрочнения на затухание силы удара главных деформаций сдвига, а также на резидуальные деформации и радиальные нормальные напряжения. Определяется одинарный параметр Gr/G для качественной спецификайии характеристик пластического и линейного упрочнения среды.